ELSEVIER

Polymer 42 (2001) 681–698

polymer

www.elsevier.nl/locate/polymer

An X-ray diffraction and modelling study of short chain branch location within the structure of polyethylene

A.M.E. Baker[1], A.H. Windle*

Department of Materials Science and Metallurgy, Pembroke Street, Cambridge, CB2 3QZ, UK

Received 4 February 1999; received in revised form 27 March 2000; accepted 12 April 2000

Abstract

The issue of whether short chain branches in polyethylene are tolerated within the crystalline component, or rejected from it, is long-standing and controversial. We have re-examined this issue by combining new X-ray diffraction techniques with molecular modelling. The X-ray diffraction patterns were recorded from a series of polyethylenes covering a broad range of branch types, contents and distributions, in both unoriented and fibre sample forms. This paper is the third and final in a sequence investigating the structure of this series. After unit cell parameters had been determined by whole pattern fitting, relative intensity ratios were measured to detect any systematic changes as functions of branch type, content and distribution. Previous studies have investigated only changes in the unit cell parameters. The influence of paracrystalline distortions was taken into account. Significant changes were found in three intensity ratios, which decreased as a function of branch concentration and increased as a function of the degree of heterogeneity (blockiness) in branch distribution. Molecular modelling showed that only branch inclusion was compatible with the experimental intensity changes. The modelling indicated that the branches were incorporated into the crystalline lattice via distortion of the neighbouring chains, mainly in the direction parallel to the unit cell *a* axis direction. The length of the branch backbone fitted into the lattice by lying approximately parallel to the unit cell *c*-axis (the main chain direction), emulating a section of a main chain.

Another finding from the modelling concerned the extent of inclusion in the more highly branched samples (typically 15–20 SCB/1000C, linear low density polyethylene). For models of these samples, branches could only be tolerated within a unit cell having the experimental values of unit cell parameters at concentrations around 3 SCB/1000C, substantially lower than in the bulk material. At higher incorporated branch concentrations, crystalline packing of the chains was not maintained during model minimisation. For such polyethylenes, branches must therefore be partitioned between the crystalline and amorphous regions. These modelling findings provide a theoretical basis for the recent, similar experimental findings from solid-state ^{13}C nuclear magnetic resonance spectroscopy.

Keywords: Molecular modelling; Branched polyethylene; Crystalline structure

1. Introduction

Most commercial grades of polyethylene contain low levels of short chain hydrocarbon branches, often ethyl, butyl or 4-methyl-1-pentene branches. The branch concentration is typically in the region of up to one branch per 80 carbon atoms along the polyethylene chains, or in more conventional terms, up to 18 short chain branches per 1000 carbon atoms (18 SCB/1000C). The branches are added to improve many of the properties of polyethylene, such as flexibility and toughness, which are demanded by its applications. The effects of adding the branches on the properties of polyethylene are well known and yet the more fundamental effect at the microstructural level is less well understood. At one extreme, if the branches do not affect the crystallisation process, then the branches will exist in equal concentrations in both crystalline and amorphous regions of the microstructure i.e. branch inclusion. At the other extreme, if the branches prevent crystalline packing of the chains then the crystalline regions will be formed solely from unbranched sections of the chains i.e. branch exclusion. The findings from investigations on the subject are diverse and both situations have been reported.

Early theories of copolymer crystallisation assumed equilibrium conditions and proposed the second of the two crystallisation extremes, namely that only one of the

* Corresponding author. Tel.: +44-1223-334321; fax: +44-1223-334300.

E-mail address: ahwl@cus.cam.ac.uk (A.H. Windle).

[1] Present address: MRC Laboratory of Molecular Biology, Hills Road, Cambridge CB2 2QH, UK.

0032-3861/01/$ - see front matter
PII: S0032-3861(00)00365-7

comonomer species was involved in crystallisation [1,2]. In branched polyethylene, which is essentially a copolymer of ethylene and a higher α-olefin, the branches were therefore assumed to be excluded from the crystallites. However, experimental evidence soon emerged that thermodynamic equilibrium was seldom achieved during crystallisation [3], thus challenging the assumption of branch rejection. Kinetic theories were then developed, which permitted limited incorporation of the comonomer unit into the crystal structure, favouring an intermediate situation of partial segregation of branches between the crystalline and amorphous components [4,5]. This intermediate situation seems intuitively most likely, whereby the branches disrupt the crystallisation process so that a degree of segregation of branches exists between the crystalline and amorphous regions. However, a theoretical basis for this has not been found.

1.1. Experimental studies

X-ray diffraction has been used traditionally in the experimental studies of short chain branch location. Such investigations have focused on the determination of the unit cell parameters and have shown an unequivocal expansion in the *a* and *b* parameters as the concentration of branches is increased [3,6–15]. The frequent conclusion made is that branches are included into the crystalline regions, their presence forcing the chains apart laterally and so expanding the *a* and *b* unit cell dimensions. The possibility that the unit cell expansion is also compatible with branch rejection has been pointed out [16], but not acknowledged widely. This alternative explanation proposes that if branches are excluded, the crystallites formed in more highly branched polyethylene will intuitively be reduced in thickness relative to those in more lightly branched polyethylene, because of the shorter methylene sequence lengths between the branch points. The surface stresses on the thinner crystallites in more highly branched polyethylenes are likely to be greater and so could conceivably cause the observed crystal lattice expansion [15,16]. This possibility of branch exclusion has been reinforced by the experimental observation that the *a* and *b* unit cell parameters of polyethylene increase linearly with the reciprocal of the lamellar thickness [17,18] although this finding and its implications regarding branch exclusion have seldom been recognised.

The influence of branch size on branch location has also provoked a broad range of opinion. From X-ray diffraction work, some studies have concluded that only methyl branches are incorporated [10,12], although, even these have been reported to be excluded [9]. Other studies have reported that branches up to at least five carbon atoms in length can be included [8].

Solid-state ^{13}C nuclear magnetic resonance (NMR) spectroscopy studies [19–29] have more recently provided new evidence on branch location from the chemical shift distributions for carbon atoms in the branches. From such spectra, methyl [22,23,25,26] branches both appear to exist in two environments, which have differing mobilities. One environment is highly mobile, proposed to be the relatively loosely packed chains of the amorphous component; the other is of restricted mobility, proposed to be either within the crystallites or at their surfaces. The studies indicate that branch inclusion does occur although from the intensities of the peaks and the sample crystallinity values, only to a limited extent, suggesting branch segregation between the amorphous and crystalline regions.

The proportion of branches included in the crystals has been estimated from such ^{13}C NMR work to be highest for methyl branches, at around 25% in a 6 SCB/1000C sample studied [22], corresponding to a crystalline concentration of 2 SCB/1000C and a segregation ratio of 11:1 between amorphous and crystalline regions. For ethyl branched samples, the proportion was estimated to be in the region of 8% [23,26] corresponding in the 17 SCB/1000C and 21 SCB/1000C samples studied to crystalline branch concentrations of 3 SCB/1000C and 6 SCB/1000C and segregation ratios of 10:1 and 5:1, respectively. The proportion of included branches is generally thought to decrease further with longer or more bulky branches. However, the trend may reverse for branches containing more than about 10 carbon atoms in length, when the branches are thought to be long enough to emulate lengths of the main chain backbones and so to cocrystallise with them [19,20,29]. A minimum may therefore exist in the crystalline incorporation ability of a branch as a function of its length.

The consensus of experimental studies concerning short chain branch location is that a significant proportion of methyl branches are included into the crystalline regions, ethyl branches are included to a low level and longer branches are primarily rejected to the crystallite surfaces or amorphous regions. The incorporation of methyl branches is generally believed to be approximately independent of the crystallisation conditions [12,22]. For ethyl and longer branches, a higher proportion is proposed to be included after quenching than after slow cooling [12] although opinions vary [26].

1.2. Theoretical studies

More recently, theoretical studies concerning branching in polyethylene have emerged [30–35]. These have mainly addressed branch inclusion by considering how branches could be accommodated within the crystalline structure of polyethylene and whether a specific molecular mechanism exists. A possible position within the unit cell for a methyl branch has been proposed [7], but it could not be extended for longer branches.

Interstitial sites [36–39] within the polyethylene chains, known as kinks, have been proposed to accommodate the branches as have substitutional sites between the polyethylene chains [40–42], known as jogs. Such sites in crystalline polyethylene arise from conformational defects where *gauche* states, (g and $\bar{g}$) occur along the main all-*trans* (t)

backbone [43]. Although the defects raise the energy of formation of the chain, they may enable subsequent incorporation of the branched chain into the crystal lattice, which would not otherwise be possible, producing a net reduction in energy. The defect sequence thought most likely to accommodate branches is $gt\bar{g}$, known as the 2g1 kink [36,44–47]. Estimates of the size of the interstice formed by a 2g1 kink suggest that it can accommodate methyl branches comfortably, is probably just large enough for ethyl branches, but certainly not for longer branches [39]. However, although the 2g1 kink is believed to be the most abundant equilibrium conformational defect in polyethylene [44], its density is estimated only to be 0.1 % [48]. The proportion of other defects types, as a possible means of incorporating longer branches, has been estimated to be negligible. When compared with the levels of branch inclusion suggested experimentally from the solid-state ^{13}C NMR studies described earlier, these defect concentrations are clearly not sufficient to account for branch inclusion.

A further method proposed for branch incorporation is that the branch is not included as a crystallographic defect but as a localised pocket of amorphous material, either within or at the surface of the crystallite [9,49,50]. Along similar lines, branches have also been proposed to segregate within crystallites to form boundaries, creating a mosaic block structure [51,52].

1.3. Molecular modelling studies

Molecular modelling represents an intermediate approach between theoretical and experimental studies since the parameter values of energy expressions used to model the behaviour of the polymer chains have been derived empirically. It has been used surprisingly rarely to investigate the inclusion of branched chains into polyethylene crystal lattices.

Napolitano et al. (1994) [53] performed a conformational search of single, isolated polyethylene chains 18 methylene units in length containing a single methyl or ethyl branch. It was assumed that the most stable conformation of these chains would be the same as the conformation which would exist in a crystalline lattice. Several polymer crystal structures have been predicted correctly in this way [54–57]. However, the intermolecular interactions produced by packing polymer chains together can lead to intramolecular distortions [58] and so to a change in chain conformation between isolated and crystalline chains. This situation is conceivable with branched polyethylene because of the additional volume of each branch which has to be accommodated.

Napolitano et al. (1994) [53] found that each branch lay perpendicular to the main chain in the lowest energy isolated chain conformation. This conformation was incorporated into a unit cell of polyethylene and the packing energy minimised by allowing the unit cell parameters to change. By comparing the minimised values of a and b unit cell parameters in the modelled unit cell, with experimentally determined values, it was concluded that only methyl branches could be tolerated in the crystalline environment; ethyl branches caused excessive unit cell expansion. However, the predicted packing of the isolated branched chains, with each branch perpendicular to the main chain, would reduce substantially or possibly eliminate the van der Waals intermolecular interactions. Intuitively, a small intramolecular distortion of the branches to force them to lie approximately parallel to the parent chain, rather than perpendicular, would enable all chains to pack more closely, increasing the intermolecular interactions and producing a net reduction in energy. Hence for branched polyethylene, consideration of both intramolecular and intermolecular interactions appears to be necessary, contrary to unbranched polyethylene [57].

1.4. This study

Unlike previous investigations of branch location in polyethylene, this study is not based on the determination and tentative interpretation of changes in the unit cell parameters as the branch content and type are varied. Instead we use the well established existence of these unit cell parameter changes to argue from X-ray diffraction theory that there must additionally be subtle changes in the intensities of the reflections, *independent of whether the branches are included or excluded* from the crystallites. We show from modelling that these intensity changes are different for the cases of inclusion and exclusion. No reports exist concerning the investigation of reflection intensities in a range of branched polyethylenes, probably because visual comparison of X-ray diffraction patterns reveals no obvious differences. Such comparisons are further obscured by the progressive broadening and attenuation of reflections in polyethylenes with higher branch contents, caused by the increased paracrystalline distortions and smaller crystallite size. In spite of these complications, intensity changes distinct from those indicative of general paracrystalline distortion are shown here to exist. The experimental and simulated changes are compared in an attempt to determine the likely location of short chain branches.

This paper is the third and final in an accompanying sequence investigating the structure of a series of branched polyethylenes. The first associated paper [59] describes the structural characterisation of the 15 commercial grades, including the effects of branch type, concentration and distribution on the crystalline unit cell parameters. The second paper [60] presents evidence from the X-ray diffraction patterns for a partially ordered component. Together, the sequence presents a comprehensive and original examination of the structure of branched polyethylene, using new methods in X-ray diffraction pattern recording and analysis and molecular modelling.

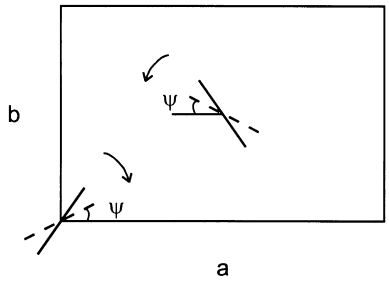

Fig. 1. Definition of the chain setting angle, ψ within the unit cell of polyethylene. The *Pnam* space group symmetry constrains the planes of the two polyethylene chains in the asymmetric unit to rotate together towards or away from the *ac* plane.

2. Theory

2.1. Central approach

For branch inclusion, a change in reflection intensities is intuitively anticipated, whether or not there is a change in unit cell parameters, because of the extra atoms inserted into the polyethylene lattice relative to the homopolymer. In the case of branch exclusion, a change in reflection intensities is less intuitive but can be demonstrated from convolution theory [61] as outlined here. The X-ray diffraction pattern, or Fourier transform of the crystal, is given by the product of the molecular transform (the Fourier transform of the unit cell motif) and the reciprocal lattice (the Fourier transform of the crystal lattice). A change in unit cell parameters of polyethylene will change the reciprocal lattice. It will also change the atomic fractional coordinates within the unit cell and therefore the molecular transform, because of the high degree of conservation of bond lengths and bond angles in polymers. Thus, both the positions and intensities of the reflections will be modified by a change in the unit cell parameters, independent of inclusion or exclusion of branches.

2.2. Interpretation of the intensity changes

Intensity changes reflect modifications in the underlying crystal structure. In the case of branch exclusion, the only structural modification possible within the *Pnam* space group symmetry of polyethylene from a change in unit cell parameters is rotation of the chains about their axes i.e. a change in the chain setting angle. The bond lengths and angles of polymers are known to be constrained tightly and therefore remain essentially constant.

The chain setting angle in polyethylene, ψ, is defined as the angle between the plane of the carbon–carbon zig-zag backbone and the *ac* plane (or alternatively the *bc* plane), as illustrated in Fig. 1. Reported values of ψ are in the range 40–50°; it is known to vary with pressure and crystallisation conditions [13,62–64]. A change in the setting angle with increasing branch concentration is plausible because of the change in the unit cell parameter *a*:*b* ratio; it is principally the *a* parameter, which expands and an accompanying gradual rotation of the plane of the carbon–carbon backbone towards the *ac* plane can be envisaged (see Fig. 1) i.e. a decrease in setting angle. The intensity changes produced by variations in the chain setting angle are predicted here by molecular modelling and compared with those seen experimentally.

For the situation of branch inclusion, molecular modelling can be used in two ways. Firstly at a fundamental level, to explore if inclusion is even possible: whether branches can be fitted in physically and tolerated within the crystalline environment of polyethylene based on the values of the unit cell parameters determined experimentally. Secondly, if tolerated, then the nature of the structural distortions incurred can be examined to determine, for example, how localised the distortion is: whether a particular chain conformation exists for accommodating a branch, such that the distortion is limited only to the branched chain, or whether the distortion is spread over the neighbouring chains.

3. Methods

3.1. Materials

Fifteen grades of commercial polyethylene were examined, which had been well characterised, as described in an associated paper [59]. In brief, the branching present in the materials had been investigated in terms of type and content by ^{13}C NMR spectroscopy and additionally, for the more highly branched grades, in terms of branch distribution (random or heterogeneous placement) by analytical temperature rising elution fractionation (TREF) [65].This sample characterisation revealed that the range of branch types was methyl (2 grades), ethyl (3 grades), butyl (1 grade), isobutyl (1 grade) and hexyl (3 grades). Furthermore, three grades contained negligible levels of branching, referred to as homopolymers, and two grades contained a mixture of short and long chain branches characteristic of LDPE (low density polyethylene). Most grades contained branch contents in the range 12–18 SCB/1000C; the highest branch content was 31 ethyl SCB/1000C. The distribution in branch placement is described by the TREF parameter $\bar{N}_w/\bar{N}_n$ [65]. A value of $\bar{N}_w/\bar{N}_n = 1.0$ indicates uniform placement of the branches along the chain backbones. Random branch placement gives values in the range 1.1–1.3, whilst higher values indicate increasing levels of heterogeneity in the branch distribution [66]. The $\bar{N}_w/\bar{N}_n$ values measured here for the more highly branched polyethylenes were in the range 1.36–1.92.

The unoriented samples were prepared by hot-pressing, with a cooling rate of 15°C min^{-1}, to a thickness of either 1.05 ± 0.03 mm or 0.80 ± 0.03 mm. Uniaxially oriented fibres were drawn from these unoriented samples to a draw ratio of 10, at a temperature of about 40°C below the melting temperature i.e. between 75–90°C depending on the

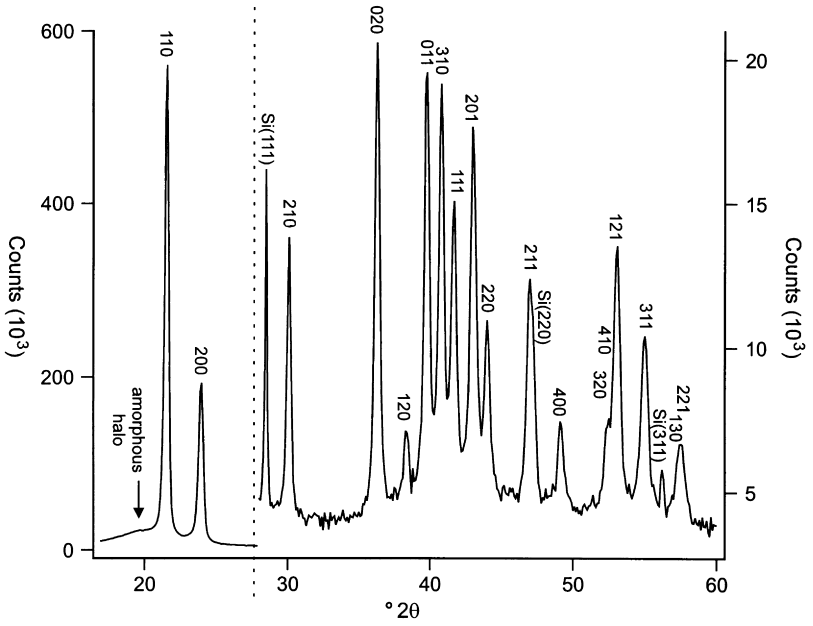

Fig. 2. Indexing of a powder diffraction pattern from unoriented high density polyethylene up to 60°2θ, containing 18 reflections. The top surface of the sample had been dusted with silicon powder and the three silicon peaks shown at 28, 47 and 56°2θ were used to aid calibration.

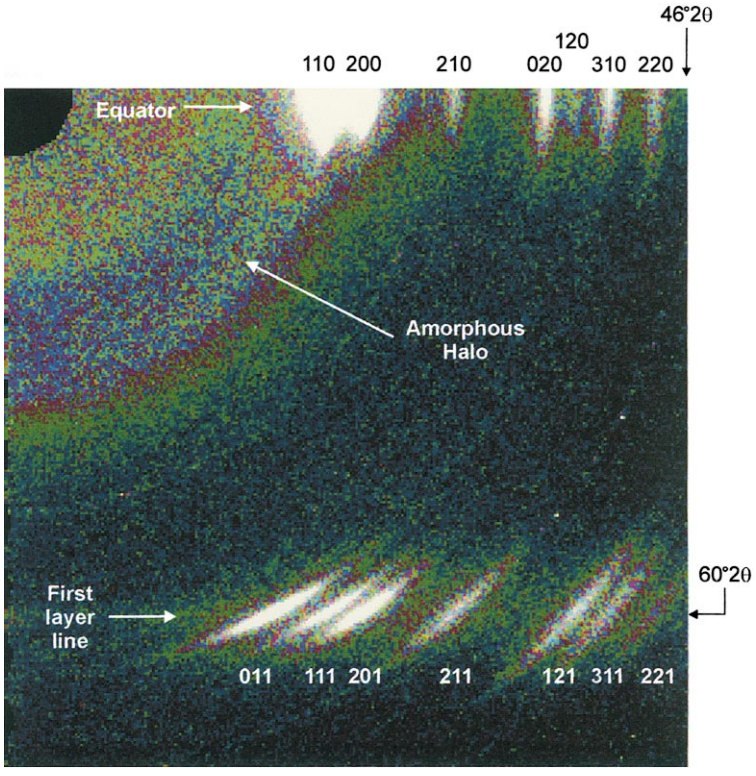

Fig. 3. Indexing of a fibre diffraction pattern from oriented high density polyethylene in the area used for peak fitting. The equator, shown up to 46°2θ contains seven reflections and the first layer line, shown up to 60°2θ also contains seven reflections. The amorphous halo around 19°2θ is very weak because the sample, a homopolymer, was highly crystalline. The colour scale goes from black (zero intensity) to white (most intense), passing seven times through the rainbow.

branch content. This consistency in sample preparation allowed confidence that any variations observed between the structures would relate primarily to chemical differences between the materials, such as the branching, rather than to differences in thermal treatment.

3.2. X-ray diffraction

Full details of the data collection methods, application of correction factors and pattern analysis methods have been given in the associated papers [59,60]; only a brief outline follows here.

X-ray diffraction patterns from the unoriented samples were recorded in reflection mode under parafocusing conditions using a Siemens D500 vertical diffractometer with a copper sealed tube source, secondary beam monochromator and scintillator counter. A sample transparency correction was made to each diffraction pattern [67]. Fig. 2 shows one of the diffraction patterns from a homopolymer HDPE sample and labels the reflection indices. After correcting for Lorentz and polarisation effects, the peak positions and intensities of the 18 reflections in the range 10–60°2θ were fitted and refined with the Rietveld method, using Philips PC Rietveld Plus v1.1B software [68]. The presence of a small degree of preferred orientation was corrected as part of the Rietveld refinement process using the March model [69]. Pseudo-Voigt profiles were used to describe the peak shapes and peak widths were fitted using the Cagliotti equation. This consistency in fitting was maintained across all the grades and enabled confidence when comparing relative intensity ratios between different samples. Some overlapping of reflections was present especially in the more highly branched grades. However, this did not present particular difficulties since the samples were pure and the structure of polyethylene is well known. Correspondingly, the reflections were not fitted independently; all the diffracted intensity had to be fitted according to one set of unit cell parameters. There were sufficient non-overlapping peaks that determination of the unit cell parameters was unambiguous. Thus even if peaks were overlapping, the positions of the component peaks were well determined. The same applied to fitting the peak widths and shapes of the overlapping reflections.

X-ray diffraction patterns from the uniaxially oriented fibres were recorded in transmission mode using a novel fibre diffractometer recently designed and built in our laboratory [70,71]. The diffractometer used a copper sealed tube source, primary beam monochromator and a scanning CCD detector. From the diffraction patterns obtained, the reflection positions and intensities were fitted and refined using a Gaussian profile with the CCP13 suite of fibre diffraction software (Daresbury Laboratory). With the fibre samples, there were fewer overlapping peaks than with the unoriented samples because the orientation present resolved the reflections into two dimensions. The area of the fibre diffraction patterns used for analysis is shown in Fig. 3. The intensities of 14 reflections were fitted, as identified in Fig. 3: seven reflections along the equator (to 46°2θ) and seven reflections along the first layer line (to 60°2θ).

To detect changes in the intensities of the reflections, intensity ratios between reflections were monitored. Visual comparison of the X-ray diffraction patterns revealed increasing paracrystallinity with higher branch content, shown by progressive broadening of the reflections and attenuation of the intensities with increasing Bragg angles. To minimise the influence of paracrystallinity, only intensity ratios between reflections with similar Bragg angles were calculated, taken to be reflections separated by up to 5°2θ. An exception was made for (210) whose nearest reflection, (020), was 7°2θ away. It was assumed that general paracrystallinity effects within this small 2θ range would be too slight to cause significant intensity changes with the statistically small number of samples used. Instead, any significant ratio changes found were assumed to be caused by branching effects, whether from inclusion or from exclusion. The ratio values were analysed as functions of sample branch content and branch distribution, for both the unoriented and fibre data.

3.3. Molecular Modelling

Molecular modelling of branch exclusion and branch inclusion in crystalline polyethylene and calculation of the corresponding X-ray diffraction patterns was performed using the CERIUS2 software developed by Molecular Simulations Incorporated (Cambridge, UK). The aim was to reproduce the X-ray diffraction intensity ratio changes seen experimentally between unbranched and branched polyethylene. For the reasons described earlier, sections of the crystalline lattices were simulated rather than adopting the single chain approach of Napolitano et al. (1994) [53] because of the anticipated importance of intermolecular as well as intramolecular interactions.

For simulating branch exclusion, the chain setting angle in a unit cell of unbranched polyethylene was varied from 0 to 90°, which covered all possibilities. The unit cell was constructed according to the unit cell parameters and atomic coordinates of Kavesh and Schultz [13]. The unit cell parameters and bond lengths and angles were fixed whilst the setting angle ψ (defined with respect to the *ac* plane; see Fig. 1) was varied in five or 10° steps. The resulting X-ray diffraction patterns were simulated up to 60°2θ for unoriented and uniaxially oriented material and the intensity ratios between each (*hkl*) reflection and the lowest angle (also the most intense) reflection, (110) were calculated. The effects of polarisation and Lorentz factors, and a graphite monochromator were included so that comparison could be made with the intensity ratio trends found experimentally.

For simulating branch inclusion, the low branch concentration typical of branched polyethylenes meant that the construction of models of the crystal lattice sufficiently

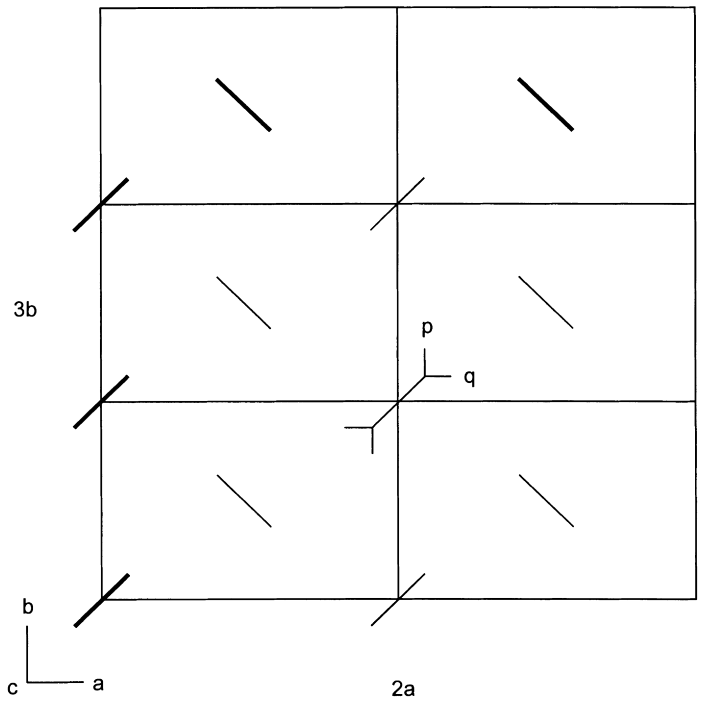

Fig. 4. The *ab* section through the model of $2 \times 3 \times 13$ unit cells used to investigate branch inclusion. Each line shows the plane of a carbon–carbon backbone of a polyethylene chain. The five outer chains shown by thicker lines were fixed during minimisation to provide stability for the model. The two possible branch locations considered are labelled *p* and *q*.

large to simulate random placement of branches was computationally not feasible. Instead, the general structural distortions incurred by branching were studied by inserting one or two branches into a section of unbranched polyethylene lattice built according to the experimentally determined unit cell parameters for the sample being examined. Unit cell parameter values for each branched polyethylene had been determined from uniaxially drawn fibres as well as unoriented samples; for the molecular modelling, the unit cell parameter values from the fibre samples were used because these samples showed a broader range of unit cell parameter values [59] and so were more likely to reveal changes in intensity ratios.

The branch contents of the samples examined experimentally ranged from 0–31 SCB/1000C; most samples contained around 14 SCB/1000C. Assuming no segregation of branches between amorphous and crystalline regions, this concentration corresponds to one branch per 18 unit cells, or one branch in a section of lattice of size $2 \times 3 \times 3$ unit cells. However, etching [50] and ^{13}C NMR studies [22,23,26] have indicated that the levels of branching present in the crystallites are lower than the overall sample branch concentration. Therefore, in addition, models were also constructed to simulate branch segregation, with lower branch concentration in the crystal models than the experimental sample being simulated. Combining the findings of ^{13}C NMR studies regarding branch segregation [19–29] (see Section 1), an approximate crystalline branch concentration was taken to be 3 SCB/1000C corresponding to a lattice size of $2 \times 3 \times 13$ unit cells (one branch per 78 unit cells) as shown in Fig. 4. The 2×3 size in the *ab* plane was chosen so that during lattice energy minimisation, the branched chain and its nearest shell of six neighbour chains could be minimised whilst the next-nearest-neighbour chain shell was fixed to provide a degree of stability.

To construct a branched lattice section for a particular sample, a polyethylene unit cell was built according to the experimentally determined unit cell parameters, preserving the known bond lengths and angles [72]. The lattice energy was minimised by varying the setting angle. A lattice section was then generated, either $2 \times 3 \times 3$ or $2 \times 3 \times 13$ unit cells. Such a section is shown in Fig. 4, which illustrates the two distinct branch locations possible, labelled *p* and *q*. Previous studies of branch energetics [32,33] showed that a methyl branch in the *q* position is slightly lower in energy than one in the *p* position. This was tested and confirmed here and subsequently branches were inserted in the *q* position to aid consistency when comparing findings. To create a methyl branch inside the lattice, a hydrogen atom at the *q* (or *p*) position on a polyethylene chain in the central portion of the lattice was converted to a carbon atom; this methyl carbon was then filled with three hydrogen atoms. All bond lengths and angles in the methyl branch were adjusted to the standard values for hydrocarbon polymers [72] according to standard carbon–hydrogen bond lengths and angles in hydrocarbon polymers. With care, this procedure did not cause a collision between the branch and its

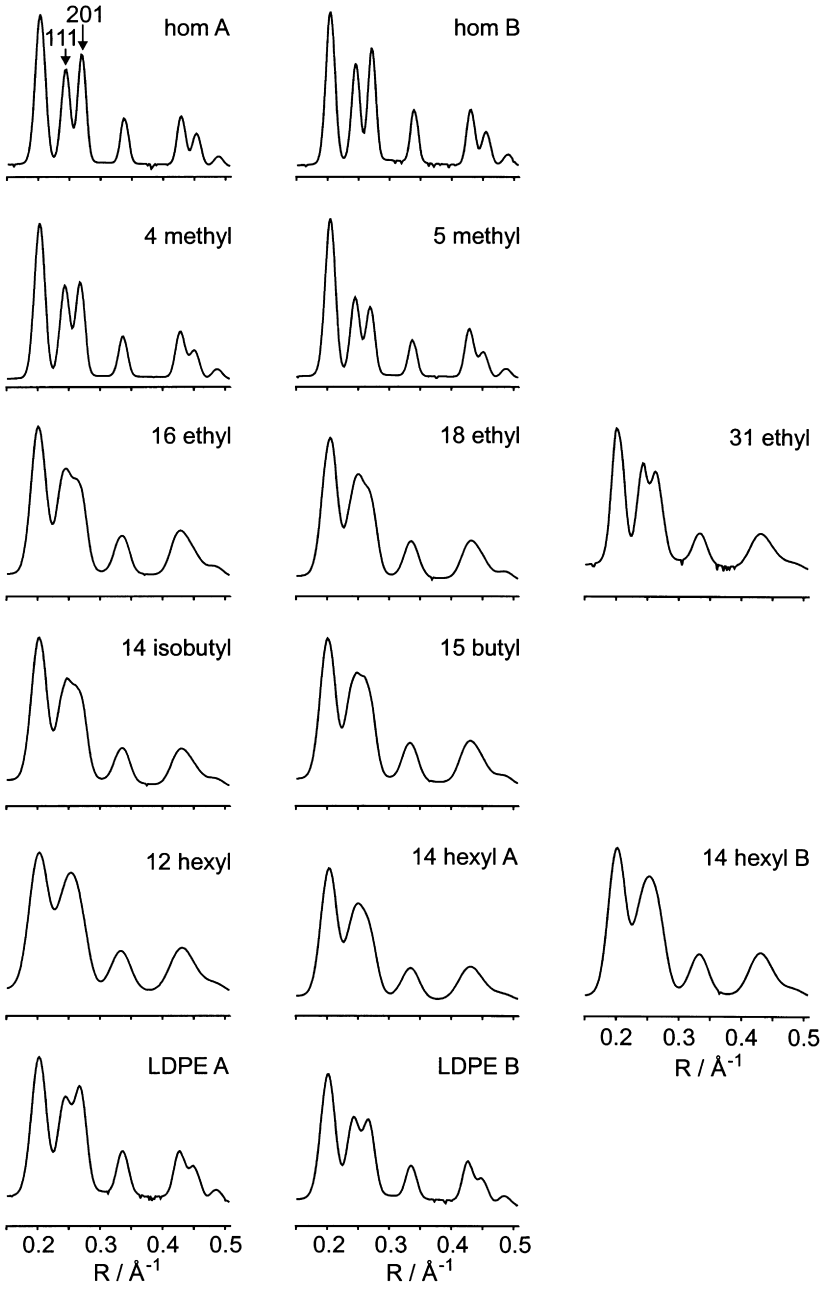

Fig. 5. The fits to the seven reflections of the first layer line (up to 60°2θ, or 0.51 Å^{-1}) of the fibre X-ray diffraction patterns for all 14 samples in oriented form. An increase in peak broadening is seen with increasing branch content and also differences in the relative intensity of the adjacent reflections (111) and (201). The sample identifiers indicate the sample branch type and number of branches per 1000 carbon atoms as used in ref. [59].

neighbouring chain. Branches up to hexyl were produced by extending this method and collisions with the neighbouring chains were avoided by adding the branch so that it lays approximately parallel to the *c*-axis, the chain direction. Constrained lattice energy minimisation was then performed using the Universal force field [73], which has been validated for organic molecules including polymers [74]. The charge equilibrium method [75], developed in conjunction with the Universal force field, was used to calculate the initial charges and to recalculate them periodically during the minimisation. The overall size of the lattice was fixed, so preserving the experimentally determined values of unit cell parameters, as were the atomic coordinates of the outer five chains and the methylene units at the ends of the seven central chains, so stabilising the lattice. The atomic coordinates of the remaining portions of the central seven chains were adjusted in order to reduce the energy of the lattice using the conjugate gradient algorithm [76]. Electrostatic charges were recalculated after every 50 cycles of energy minimisation and convergence to a RMS force of less than 0.1 kcal mol^{-1} Å^{-1}

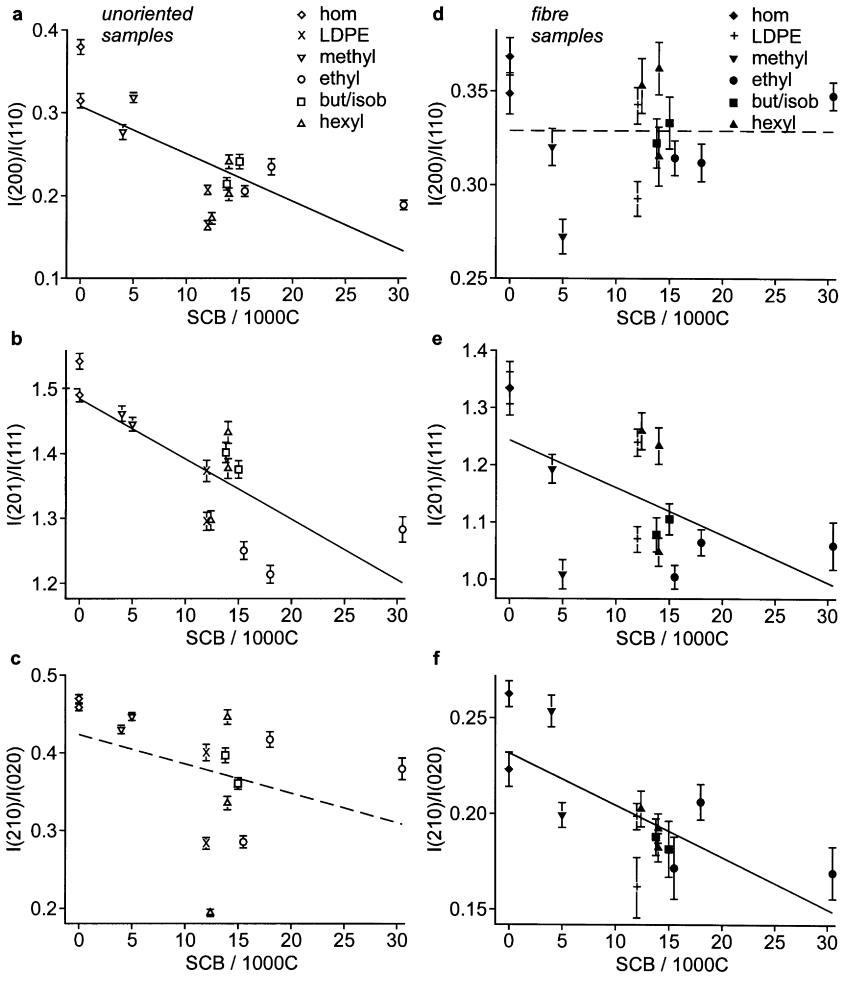

Fig. 6. The intensity ratios $I(200)/I(110)$, $I(201)/I(111)$ and $I(210)/I(020)$ as a function of branch content, determined from the experimental X-ray diffraction patterns. The linear regressions are shown by a solid line if the slope was significantly different from zero ($P < 0.05$, t-test), dotted otherwise. The three ratios show a decrease with increasing branch content.

(0.42 kJ mol^{-1} Å^{-1}) occurred typically after a few hundred cycles.

4. Results

4.1. Experimental X-ray diffraction

Visual comparison of the diffraction patterns showed progressive broadening and overlap of reflections with increased branch content, consistent with higher levels of paracrystalline distortions coupled with a reduction in crystallite size [59]. Small intensity fluctuations were nevertheless observed in the unoriented sample X-ray diffraction patterns within the collection of five reflections in the range 40–44°2θ, namely (011), (310), (111), (201) and (220). Although these five reflections became progressively more overlapped as branch content was increased, the fitting process allowed objective analysis of each peak and confirmed that the intensity fluctuations were genuine.

For the fibre X-ray diffraction patterns, visual comparison was most effective when sections through the patterns were viewed, parallel to the layer lines. The first layer line revealed a change in the ratio of the adjacent (201) and (111) reflection intensities. Intensity fluctuations in these reflections were also noted in the unoriented diffraction patterns. The change was clearer in the fibre patterns because the collection of five overlapping reflections from the unoriented sample patterns in the range 40–44°2θ was resolved into two reflections on the equator, (310) and (220), and three on the first layer line, (011), (111) and (201). The fits to the first layer line for all the fibre samples are shown in Fig. 5 where the fluctuation in the ratio of (201) and (111) intensities is seen particularly clearly between the homopolymer and methyl branched samples. Fig. 5 also illustrates the gradual broadening of reflections with increasing branch content. This broadening indicates higher levels of distortion and a reduced crystallite size, which can be argued to be consistent with models of both branch inclusion and exclusion, as described in Section 1.

After peak fitting to the reflections in the unoriented and fibre X-ray diffraction patterns, ratios of the reflection

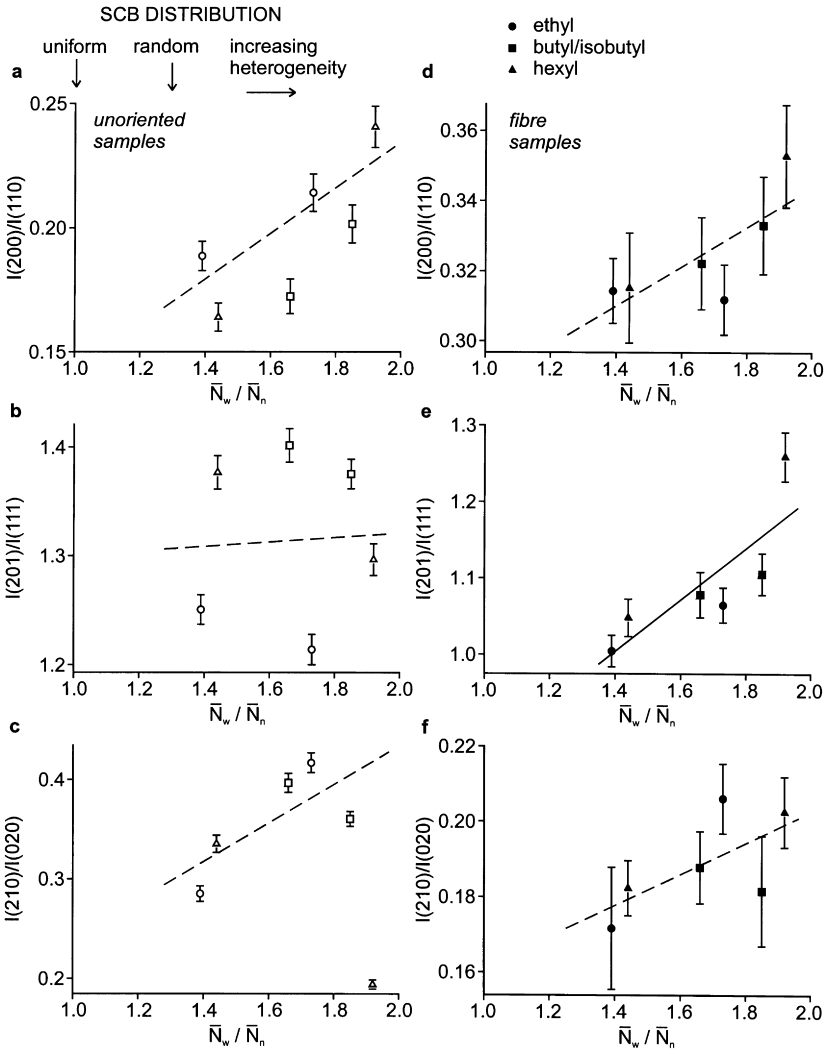

Fig. 7. The intensity ratios $I(200)/I(110)$, $I(201)/I(111)$ and $I(210)/I(020)$ as a function of branch distribution, determined from the experimental X-ray diffraction patterns. The linear regressions are shown by a solid line if the slope was significantly different from zero ($P < 0.05$, t-test), dotted otherwise. The *3* ratios show an increase with increasing heterogeneity in branch distribution.

intensities were plotted as a function of branch content, between adjacent reflections or those closely spaced in Bragg angle, within $5°2\theta$. The plots revealed significant trends ($P < 0.05$, t-test on regression slope) for three of the ratios: $I(200)/I(110)$, $I(201)/I(111)$ and $I(210)/I(020)$, as seen in Fig. 6. The reflections forming the numerator were selected such that all three ratios showed a decrease with increasing branch content. The other intensity ratios were found either not to depend on sample branch content or if trends were present, they failed to reach significance, probably because of the relatively small number of samples and the considerable scatter in their data-points. From Fig. 6, only one of the three intensity ratios, $I(201)/I(111)$, shows a significant decrease for both unoriented and fibre samples; again this is probably because of the small number of samples and their data-point scatter. Interestingly, the decrease in $I(210)/I(020)$ was counter to the trend anticipated from general paracrystalline distortions since the higher angle (020) reflection increased in intensity relative to the lower angle (210) reflection. Furthermore, (210) and (020) are separated by $7°2\theta$, whereas all other ratios examined concerned reflections separated by less than $5°2\theta$; an exception was made for (210) because of its isolation (see Fig. 2). This separation of $7°2\theta$ is large enough that effects of attenuation in $I(020)$ from general distortions may have been expected to cancel out any increase and this change is therefore a particularly robust finding.

In one of the associated papers [59], scatter within the unit cell parameters of the same set of samples was found to be correlated with variations in the branch distribution (random or heterogeneous). Similarly, Fig. 7 replots the three intensity ratios of Fig. 6 as a function of branch distribution. There are fewer data-points in Fig. 7, because the analysis of branch distribution is only valid for more highly branched polyethylenes, above about 10 SCB/1000C [65]. In addition, the branch distribution of the two LDPE grades

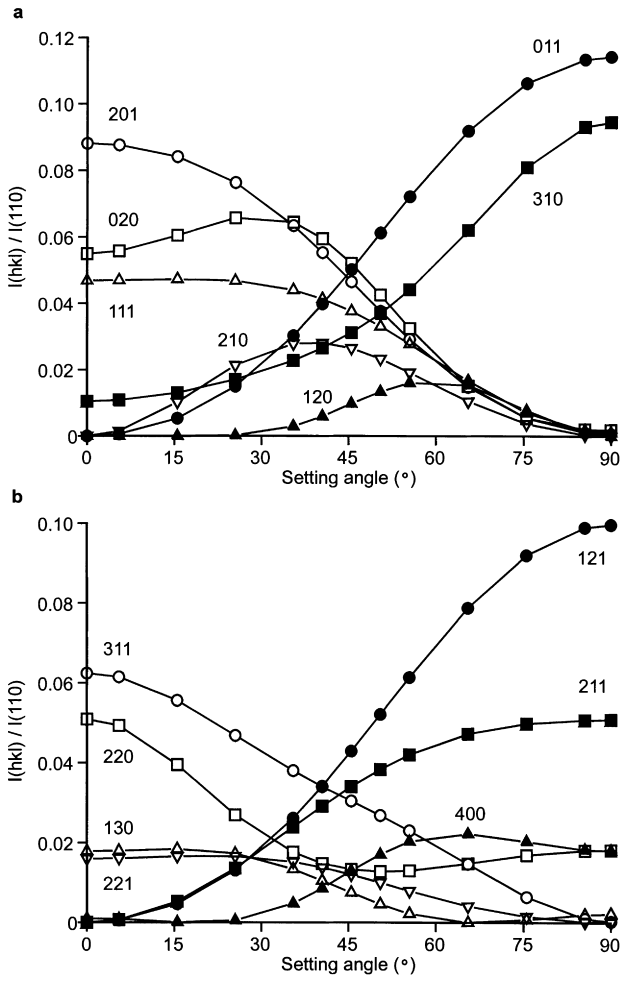

Fig. 8. The effect of setting angle on the intensity ratios $I(hkl)/I(110)$, calculated by molecular modelling. (a) Ratios involving reflections in the range 0–44°2θ. Note: the intense $I(200)/I(110)$ ratio is shown separately in Fig. 9. (b) Ratios involving reflections in the range 44–60°2θ. Note: for clarity, the ratios involving the weak (320) and (410) reflections have been omitted. The intensity ratios are seen to be most sensitive to setting angle in the region of 45° where, from experimental data, the setting angle is known to lie.

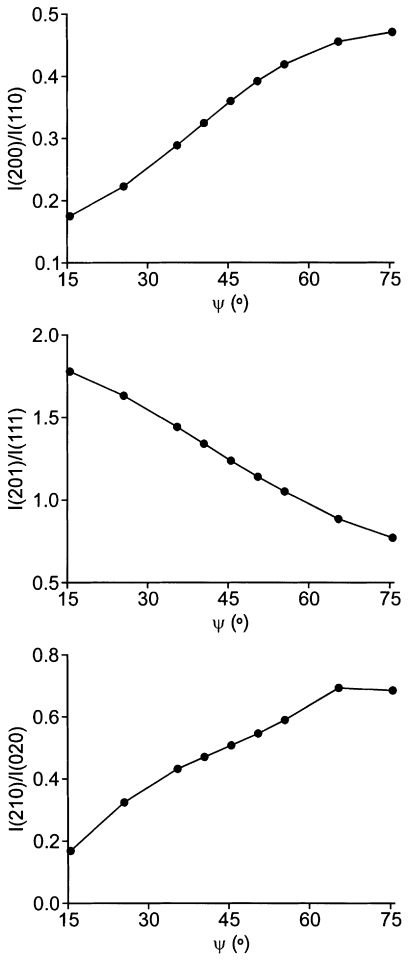

Fig. 9. Calculation from molecular modelling of the intensity ratios $I(200)/I(110)$, $I(201)/I(111)$ and $I(210)/I(020)$ as a function of chain setting angle, ψ, to investigate whether the experimental X-ray diffraction results are consistent with a model of branch exclusion. The three ratios do not all show the same trend, whether an increase or decrease with setting angle, and so the model of branch exclusion is not consistent with the experimental findings of Figs. 6 and 7.

was not known and the most highly branched sample (31 SCB/1000C) was not included in Fig. 7, because its branch content was so much higher than the rest of the data-points so that the sample was not strictly comparable regarding branch distribution. Fig. 7 shows that the largest decrease in the intensity ratios occurred for the more randomly branched samples, in the same way that these samples were found to show the largest increase in unit cell parameters [59].

4.2. Molecular modelling

4.2.1. Branch exclusion

The modelling of branch exclusion via a change in chain setting angle of the crystalline unbranched chains showed that the reflection intensities in the X-ray diffraction pattern of polyethylene are very sensitive to the value of the setting angle. To gain an overall understanding of the setting angle effect, the reflection intensity values were first scaled with respect to the dominant, lowest angle (110) reflection and plotted as a function of the chain setting angle, as shown in Fig. 8 for unoriented material. The intensity ratio trends found as function of setting angle were tested and confirmed to apply across the range of unit cell parameters recorded. The plot for fibre sample geometry showed the same trends, but the intensity ratio values were all higher. This was expected since (110) is the lowest Bragg angle reflection of polyethylene and, in reciprocal space, the three-dimensional spherical shell of (*hkl*) reflection intensity from unoriented (powder) sample geometry becomes concentrated into a two-dimensional (2D) circular shell for fibre geometry. Fibre diffraction intensities of higher angle reflections are therefore relatively strong with respect to (110), compared with the equivalent unoriented diffraction pattern.

Table 1
Description of the models built to examine branch inclusion and values from these models of the three intensity ratios found to change in the experimental X-ray diffraction work of Figs. 6 and 7. All branches were added in the *q* position (see Fig. 4). The second column shows the branch content and type of the experimental sample which each model represents: the model unit cell parameters were fixed to the values determined experimentally for these samples

Branch type	Exptl sample modelled	Lattice size of model	No of branches in model	Equiv. SCB/1000C	$I(200)/I(110)$	$I(201)/I(111)$	$I(210)/I(020)$
None	Hom	$1\times1\times1$	0	0	0.365	1.273	0.495
Methyl	5 methyl	$2\times3\times13$	1	3 methyl	0.362	1.280	0.496
Methyl	5 methyl	$2\times3\times13$	2	6 methyl	0.354	1.272	0.481
Ethyl	18 ethyl	$2\times3\times13$	1	3 ethyl	0.353	1.266	0.463
Butyl	15 butyl	$2\times3\times13$	1	3 butyl	0.349	1.324	0.482
1,5-dibutyl	15 butyl	$2\times3\times13$	2	6 butyl	0.317	1.259	0.471
Hexyl	14 hexyl	$2\times3\times13$	1	3 hexyl	0.331	1.226	0.458

Only seven of the reflection ratios from the reflections up to $44°2\theta$ are shown in Fig. 8a for reasons of clarity; the anomalously high $I(200)/I(110)$ ratio is shown separately in Fig. 9. Many of the intensity ratios in Fig. 8 show a sigmoidal dependence with setting angle, with maximum and minimum values at setting angles of 0 and 90°, for example $I(011)/I(110)$. These intensity ratios are therefore most sensitive to changes in the setting angle at around 45°, where the setting angle in polyethylene is known to lie [13,64]. This is also its value in paraffins [62] and extended chain polyethylene [63]. A few intensity ratios showed a maximum at an intermediate value of setting angle, such as $I(210)/I(110)$. Examination of intensity ratios should thus provide a sensitive method of estimating the chain setting angle, at least for unbranched polyethylene. By comparing Fig. 8 with values from the experimental diffraction patterns, the setting angle here for the homopolymer grades was estimated to lie in the range 44–47°.

Fig. 8 demonstrates that even a small change in chain setting angle produces changes in reflection intensity values, which are large enough to be detected experimentally (compare the scale and error bars of Fig. 6 with Fig. 8). Thus a change in the setting angle has the potential to cause the intensity ratio changes seen experimentally in Fig. 6. Fig. 8 predicts whether a particular ratio will increase or decrease as a function of setting angle and so it can be used to investigate whether the intensity ratio trends found experimentally as a function of branch content are consistent with a change in setting angle. To examine this, the three ratios found to change experimentally, namely $I(200)/I(110)$, $I(201)/I(111)$ and $I(210)/I(020)$, were calculated from the simulation data of Fig. 8 and are plotted in Fig. 9. If a change in chain setting angle were consistent with the experimental data of Fig. 6, then all three ratios in Fig. 9 should show the same trend, whether an increase or a decrease, in the same way that the three ratios of Fig. 6 show the same trend with branch content (or branch distribution in Fig. 7). However, Fig. 9 shows that $I(200)/I(110)$ and $I(210)/I(020)$ both increase as setting angle increases but $I(201)/I(111)$ shows a decrease. We therefore conclude that a change in setting angle with increasing branch content is not consistent with the intensity trends found experimentally.

4.2.2. Branch inclusion

Crystal models containing levels of branching typical of the commercial samples examined experimentally, namely around 15 SCB/1000C, were found to be unstable during energy minimisation and the chains failed to retain crystalline packing. When the branch concentration in the models was reduced, however, to around the level reported for the crystalline component of similar branched polyethylenes by solid-state ^{13}C NMR spectroscopy [22,23,26], namely around 3 SCB/1000C, then stable minimisations resulted, which retained crystalline packing of the chains.

Table 1 shows details of six models, which successfully retained crystalline packing after minimisation; a homopolymer model is included as a reference. All branches had been placed in the *q* position (see Fig. 4). The unit cell parameter values used in the models were those determined experimentally from the samples listed in the second column. Among the six models is one containing two butyl branches in the form of a 1,5-dibutyl unit. Such bunching together of branches caused by inhomogeneity in the branch distribution is known to occur in branched polyethylenes [77,20]. The 1,5-dibutyl branch model was included to examine the possibility of multiple branch entities being included into the crystalline material of polyethylene, as well as the single branches.

Examination of the minimised models revealed several common features. These are illustrated in Fig. 10, which shows the model from Table 1 containing a single butyl branch after minimisation. The branch concentration is one butyl branch in $2\times3\times13$ unit cells of polyethylene, equivalent to 3 SCB/1000C; the starting model was like that shown in Fig. 4. Fig. 10a shows the view looking down the unit cell axis parallel to the chain axis (the unit cell *c*-axis). It is seen how minimisation was confined to the branch containing parent chain and its nearest six neighbouring chains whilst the outer five chains were fixed. The close packing of the chains has been retained with the end section of the butyl branch attempting to mimic the backbone positioning of the adjacent row of chains. The distortion in the minimised chains is predominantly parallel to the *a*-axis direction, as seen by comparing Fig. 10b and c. Fig. 10b reveals a tightly packed "honeycomb" structure in the *bc* plane; the chains are relatively undistorted and the chain

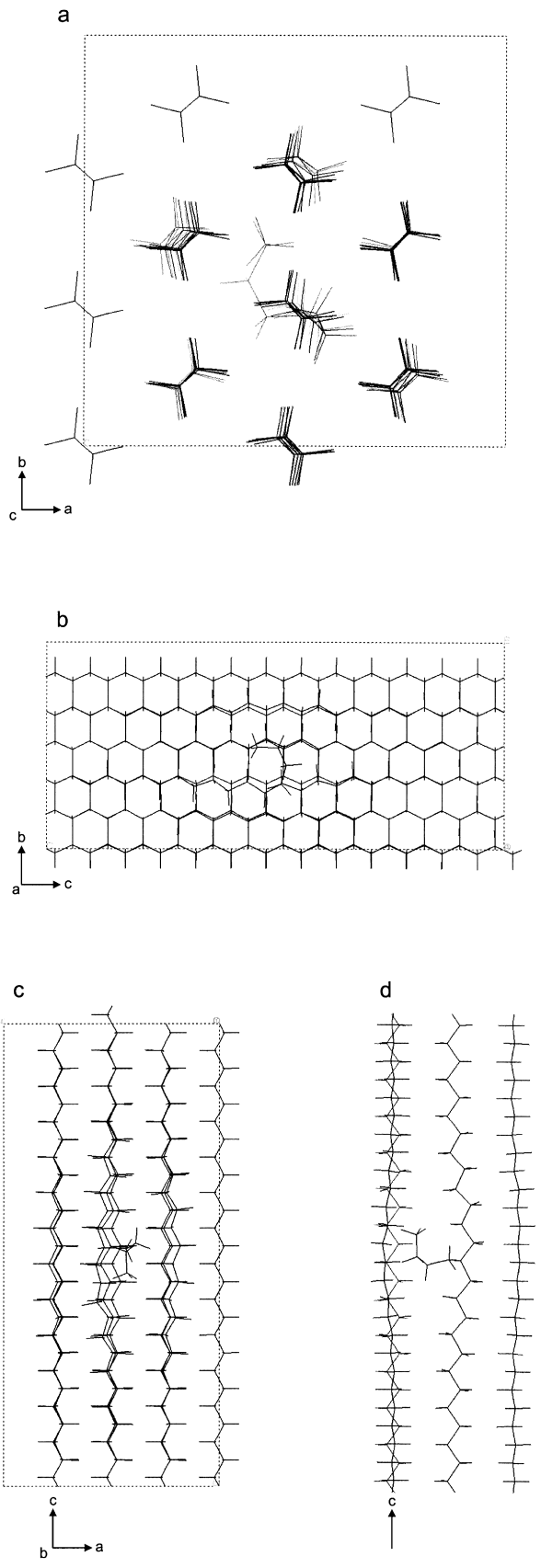

Fig. 10. Four views from molecular modelling of a minimised structure containing a butyl branch. (a), (b), (c): views down each of the three unit cell axes; (d) and an off-axis view containing the *c*-axis.

backbones return to their original positions only a few methylene units away from the branch point. Fig. 10c reveals a more open section in the *ac* plane, with the chains accommodating considerable distortion in the region of the branch point. Together with Fig. 10d, the branch end is seen to mimic the positioning of the main backbone chains: the first two methylene units of the branch protrude approximately perpendicular to the parent chain and the rest of the branch turns to lie approximately parallel to the main chain backbone. Similar branch positioning was noted for the models containing a hexyl branch. For models containing the shorter methyl and ethyl branches, the positioning of the minimised branch was less specific; in general, it was approximately perpendicular to the parent chain, like the first two methylene units of the butyl branch in Fig. 10.

The distortion seen in Fig. 10 and in all the minimised branch-containing lattices was concentrated along the *a*-axis direction. Diffraction theory shows that distortion in a crystal lattice reduces the reflection intensities with the "lost" part of the scattered intensity appearing instead as part of the background [78,79]. From this, it might be expected that as branch concentration is increased in polyethylene, those (*hkl*) planes, which are approximately normal to the *a*-axis and therefore have the greatest distortion from incorporated branches, should show a reduction in diffracted intensity relative to the other (*hkl*) reflections. Thus (*hkl*) reflections where *h* is non-zero and especially where it is the largest of the three (*hkl*) indices, should show a reduction in intensity relative to reflections where *h* is zero or a low integer compared with *k* and *l*. This supposition was difficult to investigate extensively from modelling because of practical constraints such as lattice size limitations and the number of models which could realistically be set up and run. A full investigation of (*hkl*) intensity changes according to branch type and branch concentration was therefore not possible in this study. Instead, the above hypothesis was investigated by comparing the reflection intensity ratios from minimised unbranched and minimised branched polyethylene models.

From each minimised model, values were calculated for the three intensity ratios found to change experimentally; these are shown in Table 1. To test whether the insertion of branches produced a statistically significant change in these intensity ratios, a paired *t*-test was performed for each ratio between the value for the unbranched model and the values for the branched models. In addition, all other intensity ratios between reflections separated by less than $5°2\theta$, excluding the weakest reflections such as (120) and (320), were calculated from the models and similar paired *t*-tests performed. The results for these 20 ratios are shown in Table 2. The direction of change from the unbranched to branched models, whether an increase or decrease, was determined for each ratio. This change was then compared with that predicted by a model of isotropic distortion, in which the intensity ratio between a reflection at a higher Bragg angle to a reflection at a lower Bragg angle will decrease. These calculations investigated whether the

Table 2
Listing of (*hkl*) intensity ratio values from the molecular modelling work of branch inclusion, between unbranched and branched polyethylene (columns 2 and 3, respectively) and the magnitude and direction of the change (column 4). Column 5 indicates the three ratios found experimentally to decrease as the branch content was raised (see Figs. 6 and 7); these three ratios are also labelled [ex] in column 1. For further comparison with columns 4 and 5, column 6 lists the ratio changes predicted by isotropic distortion (paracrystallinity). Similarly, column 7 lists the changes predicted by the model of branch exclusion where a decrease in chain setting angle from around 45° was anticipated with increasing branch content (refer to Fig. 8). The 20 ratios concern reflections within 5°2θ and have been calculated from the minimised models of Table 1. The last four ratios concern reflections with the same *h* index, which would be expected to show relatively little change on the basis of the *a*-axis chain distortion hypothesis. The table demonstrates that the branch inclusion models are reasonably consistent with the experimental changes, unlike the models of isotropic distortion and branch exclusion. *sd*, standard deviation. * indicates significance of the change, $P < 0.05$, ** for $P < 0.01$

hkl Intensity ratio	Ratio value		% Change from unbranched to branched model	Changes (signif.) from experimental XRD	Change if isotropic distortion	Change if decrease in setting angle from 45°
	Unbranched model	Branched models mean ± sd				
200/110[ex]	0.365	0.344 ± 0.017	−5.8*	−	−	−
210/020[ex]	0.495	0.475 ± 0.014	−4.0*	−	+	−
310/020	0.594	0.536 ± 0.040	−9.8*		−	−
310/011	0.661	0.622 ± 0.037	−6.0*		−	+
111/011	0.740	0.753 ± 0.025	+1.8		–	+
201/011	0.943	0.959 ± 0.040	+1.7		−	+
220/011	0.299	0.303 ± 0.016	+1.3		–	+
310/111	0.892	0.826 ± 0.048	+1.3		+	–
310/201	0.701	0.650 ± 0.035	−7.3*		+	−
310/220	2.21	2.06 ± 0.13	−7.1*		+	−
201/111[ex]	1.273	1.271 ± 0.032	−0.2	−	−	+
220/111	0.403	0.402 ± 0.018	−0.2		−	−
400/220	0.95	0.78 ± 0.11	−17.1*		−	−
400/211	0.423	0.364 ± 0.033	−13.9**		−	+
400/121	0.342	0.286 ± 0.028	−16.4**		+	+
311/121	0.728	0.710 ± 0.021	−2.5		+	+
011/020	0.899	0.862 ± 0.030	−4.1*		−	−
220/201	0.317	0.317 ± 0.010	−0.2		−	−
211/201	0.707	0.677 ± 0.023	−4.2*		−	−
211/220	2.23	2.14 ± 0.12	−4.0		−	−

intensity changes predicted were consistent with the hypothesis of most distortion being accommodated parallel to the *a*-axis and if so, whether other intensity ratios might also have been expected to show a change experimentally.

Table 2 lists 20 intensity ratios between reflections separated by less than 5°2θ, excluding the weakest reflections. The first 16 ratios concern reflections with different *h* indices; the numerator reflection has the higher *h* index so that a decrease is anticipated based on the *a*-axis chain distortion hypothesis. The value from the unbranched model is shown in the second column followed by the average and standard deviation of values from the six branched models of Table 1. The percentage difference and its sign relative to the unbranched model is shown in the fourth column, with * and ** indicating statistical significance. Ten of the 16 ratios show significant changes, including two of the three ratios found to change in the experimental X-ray diffraction study: $I(200)/I(110)$ and $I(210)/I(020)$. The sign of the change anticipated on the basis of isotropic distortion is shown in the penultimate column. The 10 significant ratio changes from the models of branch inclusion are all decreases, consistent with the *a*-axis distortion hypothesis, and, even more powerfully, the decrease in five of these ratios is in direct contrast with the increase expected from a model of general, isotropic distortion. This demonstrates that the models of branch inclusion do not show isotropic but rather anisotropic distortion. To complete the comparison of experimental and modelled intensity ratio changes, the final column in Table 2 lists the sign of the change anticipated from the model of branch exclusion (Figs. 1, 8 and 9). It was supposed in the model of branch exclusion that the setting angle decreases steadily from around 45° as the branch content is increased; this can be envisaged from the known increase in *a*/*b* unit cell parameter ratio with branch content. As demonstrated more extensively in Fig. 9, the experimental ratio changes are not consistent with those of a decrease in chain setting angle.

The last four ratios in Table 2 concern reflections with the same *h* index. On the basis of the *a*-axis distortion hypothesis, relatively little change in these ratios is anticipated, other than a small decrease on the basis of paracrystallinity since the numerator reflections have been chosen to have the higher Bragg angle. All four ratios do indeed show a small decrease. For two of the ratios, the decrease was significant although these two ratios concerned more widely separated reflection pairs and so this is less surprising.

To summarise all the results, the intensity trends from molecular modelling of branch inclusion were consistent with the intensity trends seen experimentally, unlike the trends predicted by isotropic distortion and branch exclusion. The branches were found to be incorporated into the crystalline lattice by distortion of chains predominantly along the *a*-axis direction.

5. Discussion

5.1. Experimental X-ray diffraction

Analysis of the unoriented and fibre X-ray diffraction patterns from a broad range of branched polyethylenes has revealed significant changes in three intensity ratios as functions of both branch content and branch placement: $I(200)/I(110)$, $I(201)/I(111)$ and $I(210)/I(020)$. This is the first report concerning changes in the intensities of reflections in polyethylene although many reports exist concerning the well-known changes in unit cell parameters as a function of branch content. The reason for this is undoubtedly that the diffraction patterns from different polyethylenes look very similar except for overall deterioration in the quality of the diffraction pattern because of increased paracrystallinity as the branch content is raised. Also, the X-ray diffraction patterns are sensitive to the effects of prior mechanical and heat treatments on the polyethylene. This sensitivity further impairs quantitative comparison of the X-ray diffraction patterns. In this study, all these effects were accounted for, by consistency in sample preparation techniques, careful diffraction pattern recording and comprehensive data analysis, including the use of appropriate but rarely used correction factors [59].

There are several likely reasons why only three ratios showed significant changes in the experimental X-ray diffraction data. First, there was considerable scatter in the data-points (see Figs. 6 and 7), which may have obscured trends present in other ratios. Second, ratios from the fibre samples, which compared reflections from different layer lines showed considerably more variability than ratios which compared reflections from the same layer line. Indeed, none of the three experimentally significant ratio changes concerned reflections from different layer lines. This was a consequence of limitations in the fitting of the fibre patterns. Third, peak overlap in the more heavily branched grades caused increasing scatter and uncertainty in the peak intensity values. The fibre samples had fewer overlapping peaks than the unoriented samples because the orientation present resolved the reflections into 2D. However, the fibre sample overlap was still severe because the reflections were broader because of strain introduced by the drawing process. The extent of peak overlap in the fibre samples can be seen in Fig. 5. Nevertheless, such overlapping reflections could be fitted with reasonable certainty because the samples were pure and the structure of polyethylene is well known. The reflections were not fitted independently; all the diffracted intensity within a particular sample, whether unoriented or oriented, was fitted according to one set of unit cell parameters. There were sufficient non-overlapping peaks that determination of the unit cell parameters was unambiguous. Thus, when overlapping peaks were present the positions of the component peaks was well determined. The same applied to fitting the peak widths and shapes of overlapping reflections. The combination of these reasons probably explains why many of the other ratios, which showed a change in the modelling data in Table 2 did not also show a change experimentally. For example, five of the modelling ratios, which show a change in Table 2 concern (310). In unoriented polyethylene, (310) is the most overlapped reflection, with a reflection less than $1^\circ 2\theta$ away on each side. Three of the other modelling ratios, which changed concerned (400); this is a weak, higher angle reflection, which was not part of the measurement area for the fibre patterns (Fig. 3).

Diffraction patterns were recorded from both unoriented and fibre samples not only to increase the data available but additionally because of the advantages in the data available specific to each sample type, as just discussed. There were also differences seen between the unoriented and fibre diffraction data. One difference concerned the size of the decrease in each of the three intensity ratios, which reached significance as functions of increasing branch content and increasing heterogeneity in branch placement: the decrease was smaller across the fibre samples than across the unoriented samples (Figs. 6 and 7). Trends in the intensity ratios for the fibre samples were additionally less clear because of the higher uncertainty associated with each value. However, the decrease in all the intensity ratio plots of Fig. 6 is seen more clearly when the homopolymer HDPE data-points are compared with the branched sample data-points. The scatter in data-points is located largely between the more highly branched samples. This is seen clearly particularly in Fig. 6c where the decrease in $I(210)/I(020)$ did not reached significance, in spite of the large decrease between the homopolymer and branched polyethylene samples, probably because of the considerable scatter in the LLDPE sample data-points around 15 SCB/1000C. Fig. 7 reveals that this scatter within the LLDPE data-points in Fig. 6 was not random but correlated to the branch distribution of each sample; relative to the homopolymer samples, a larger decrease in the intensity ratio was seen for the more randomly branched samples.

This result concerning the origin of the scatter in data-points can be interpreted further by the modelling findings. The modelling showed that the experimental X-ray diffraction intensity decreases were consistent with branch inclusion. From this, Fig. 7 indicates that more branch inclusion will occur with randomly placed branches than with heterogeneously placed ones. For a given branch concentration, either more branches in a randomly branched sample are included into the crystalline material or randomly placed

branches in the crystallites cause more disruption than the same concentration of heterogeneously placed branches. The former appears more likely since the majority of branches even in heterogeneous polyethylenes are essentially isolated because of the very low concentrations and so would cause similar extents of crystalline distortion. The findings are consistent with those in an associated paper [59] where it was proposed from unit cell parameter measurements that for a fixed branch content, a higher proportion of randomly placed branches are included in the crystalline material than heterogeneously placed branches.

The decrease seen experimentally in $I(210)/I(020)$ with increasing branch content was contrary to the effect expected from general isotropic distortion within the structure. The decrease was even more surprising since the (210) and (020) reflections are relatively widely separated, by $7°2\theta$, and so are not as close in Bragg angle as the other ratios considered. Any increase had been anticipated to be cancelled out by the attenuation from paracrystalline distortions. The model of branch inclusion, however, has been shown to be consistent fully with this apparent anomaly.

5.2. Molecular modelling

The molecular modelling studies were not performed independently from the experimental X-ray diffraction results because the models were constrained to have the unit cell parameter values determined experimentally. Regarding branch inclusion, this allowed examination of whether branches could be tolerated within the crystal lattice according to crystallographic parameters determined experimentally. The modelling showed that the experimental X-ray diffraction data were consistent with branch inclusion and not consistent with branch exclusion. Before discussing the branch inclusion work further, including its limitations, the reasons for rejecting the model of branch exclusion will be discussed.

5.2.1. Branch exclusion

The branch exclusion model was based on the argument that if all short chain branches were excluded from the crystalline regions of the polyethylene samples then the experimental intensity ratio changes must have arisen from a change in the chain setting angle of the planar zigzag backbone within the polyethylene unit cell. The setting angle was assumed to change systematically with branch content. The molecular modelling demonstrated that the decreases found experimentally in the three ratios were inconsistent with those of a change in chain setting angle; the modelling data of Fig. 9 could not explain the experimental data of Figs. 6 and 7. In addition, Figs. 8 and 9 showed that if the chain setting angle was varying systematically with branch content, then other ratios should have been found to change more strongly than the three found experimentally, for example, ratios involving the (011) reflection, such as $I(011)/I(020)$ or $I(011)/I(111)$. The combination of inconsistency between the experimental and modelled intensity trends of Figs. 6, 7 and 9 and the absence of predicted larger changes in several other ratios experimentally means a change in chain setting angle cannot explain the results. Thus branch exclusion, which could in theory produce the changes seen experimentally in unit cell parameters and so conceivably also a change in setting angle, does not appear to be able to account for the experimental changes observed in the intensity ratios.

5.2.2. Branch inclusion

Objective interpretation of the simulations of branch inclusion in polyethylene was not straightforward as in the case of branch exclusion because of necessary shortcomings in the method used to model this complex situation. The crystalline lattices simulated were not representative of a random but rather of a uniform copolymer, with the same branch positions and conformations repeating infinitely throughout the structure: this is clearly unrealistic. The scatter found in the reflection intensity values in Table 2 was thought to reflect limitations such as these in the models. Thus, although one model could not accurately simulate all the structural consequences of branch inclusion, it was felt that overall features found common to all models would be realistic.

The general molecular mechanism for branch inclusion was distortion of the parent and neighbouring chains such that the branch was accommodated as a section of an additional main chain. The greatest distortion in the parent chain existed along the *a*-axis direction and was most severe at the branch attachment point where the parent chain was effectively displaced, approximately parallel to the *a* axis. The neighbouring chain backbones bent around the branch by distorting also mainly along the *a*-axis direction and gradually returned to their undistorted position over a distance of several methylene units. It was evident from Fig. 10 that the chains were most flexible in the unit cell *a* direction and this was not surprising: the *a* parameter is considerably larger than *b*. This mechanism indicates that there is intrinsically no upper limit to the length of branch, which may be incorporated into the crystalline lattice of polyethylene although clearly the energy penalty of incorporation of longer short chain branches steadily increases. This positioning of the branch is in contrast to the predictions of Napolitano et al. (1994) [53], where the entire branch was predicted to protrude at right angles from the main chain backbone. Fig. 10 illustrates clearly the importance of including interchain interactions in such simulations.

This *a*-axis distortion hypothesis can be thought of as a particular case of paracrystallinity. The paracrystallinity predictions in Table 2 assumed isotropic distortions. As shown in Table 2, five of the 10 ratios, which showed a significant decrease in the branch inclusion modelling data and one of the three ratios, which showed a change from the experimental X-ray diffraction data, would have been expected from a model of isotropic paracrystalline distortions

to show instead an increase. In fact, these discrepancies can be interpreted alternatively as indicating anisotropic paracrystalline distortions in branched polyethylene. Consistent with this, from paracrystalline theory [78], the extent of lattice distortion in crystalline polyethylene has been proposed to be much lower parallel to the main chain backbone than perpendicular to it [13,80].

The limitations of the modelling meant that a study of the effect of branch concentration in the crystalline component on the change in intensity ratio values was not possible; only differences between crystalline polyethylene models containing some and no branches are possible. A hint of the effect of branch concentration is seen, however, by comparing the intensity ratio values in Table 1 from the homopolymer model, the model containing one butyl branch and the model containing the 1,5-dibutyl branch. In agreement with the experimental findings, each of the three intensity ratios shows a clear decrease as the branch concentration increases.

An apparent discrepancy between the experimental data and those of the models of branch inclusion is the number of intensity ratios which showed a significant change with increasing branch content. The branch inclusion modelling data summarised in Table 2 showed significant changes in 10 intensity ratios, whereas experimentally significant changes were found in only three. As has already been discussed, it was argued that the figure of three intensity ratios showing a change from the experimental studies was likely to be an underestimate, principally because of the scatter in data-points. However, the 10 ratios in Table 2 are not likely to be definitive nor necessarily fully representative of the changes to be anticipated experimentally from branch inclusion. With more extensive and comprehensive modelling, the list of 10 ratios would probably change although it is anticipated always to contain ratios, which show a reduction in higher *h* index reflections relative to lower *h* index reflections, as is seen to be the case with the data in Table 2.

A further limitation of the current modelling study is the exact extent to which branches are partitioned between the crystalline and amorphous components. The figure from the modelling for the more highly branched polyethylenes (LLDPEs) of only 3 SCB/1000C being able to be incorporated successfully into the crystalline component, according to the experimentally determined unit cell parameters, rather than the bulk sample values of typically 12–18 SCB/1000C should not be regarded as a definitive value. It should be realised to be only a guide but nevertheless providing a theoretical basis for the recent similar experimental findings by solid-state ^{13}C NMR [22,23,26].

6. Conclusions

This work has combined X-ray diffraction and molecular modelling in a fresh approach to investigating short chain branch location in polyethylene. The specific aim was to determine whether the branches are excluded from or included in the crystalline regions. Previous research has studied the changes in unit cell parameters of polyethylene as the branch concentration is varied, but without success since the interpretation of the findings is ambiguous. We have used diffraction theory to show that in addition to the changes in unit cell parameters, there must be an accompanying change in the diffraction intensities, and from molecular modelling we have demonstrated that the intensity changes are different for the two possibilities of branch inclusion and branch exclusion. Experimentally, changes were indeed found in some reflection intensity ratios, and were demonstrated to be distinct from the effects of paracrystallinity. The changes involved the decrease of a high *h* index (*hkl*) reflection with respect to a lower *h* index reflection, for increasing branch content and increasing degree of randomness in branch distribution. The experimental intensity changes were inconsistent with the intensity changes predicted by modelling of branch exclusion but were in general agreement with those of the branch inclusion models. The distortion incurred in the inclusion models was concentrated along the *a*-axis direction, so explaining the reduction in intensity of high *h* index reflections found experimentally. Additionally, the modelling has shown that branch inclusion is possible only for low branch concentrations, generally lower than the overall sample concentration. This indicates partial segregation of branches with a higher density of branches in the amorphous compared with the crystalline component, consistent with recent findings by solid-state ^{13}C NMR.

This paper is the final in a sequence of three, which together present a comprehensive and original examination of the structure of branched polyethylene [59,60]. Although many other studies on polyethylene structure exist in the literature, a strength of this investigation is that it applied a considerable range of techniques to a single sample set. Furthermore, particular care was taken with the quantification of the X-ray diffraction patterns. Uniquely, interpretation of these patterns was aided by molecular modelling, a combination of approaches, which does not appear to have been used previously for polyethylenes. Our study has yielded three main conclusions. Firstly, we have shown that branch distribution (random *versus* heterogeneous) can affect unit cell parameters. Secondly, we have seen evidence in the X-ray diffraction patterns for the existence of a partially ordered component, intermediate between crystalline and amorphous forms. Finally, we have demonstrated that short chain branches can be included into the crystalline component, albeit only to a limited extent.

Acknowledgements

The authors wish to thank BP Chemicals for the TREF analysis, Mary Vickers for discussions, Simon Hanna for

advice concerning the fibre X-ray diffractometer, Chris Frye for supplying the materials and Brain Seymour, John Carter, Keith Page and Joe Ellis for technical support. The fibre diffraction patterns were analysed using the CCP13 suite of programs (CCLRC Daresbury Laboratory) and advice from Richard Denny and Gabriel Welsh is gratefully acknowledged. The work was supported by an EPSRC Research Studentship and CASE Award from BP Chemicals (AMEB).

References

[1] Flory PJ. J Chem Phys 1949;17:223.
[2] Flory PJ. Trans Faraday Soc 1955;51:848–57.
[3] Eichhorn RM. J Polym Sci 1958;31:197–8.
[4] Gornick F, Mandelkern L. J Appl Phys 1962;33:907.
[5] Helfand E, Lauritzen JI. Macromolecules 1973;6:631–8.
[6] Walter ER, Reding FP. J Polym Sci 1956;21:557–9.
[7] Cole EA, Holmes DR. J Polym Sci 1960;46:245–56.
[8] Swan PR. J Polym Sci 1962;56:409–16.
[9] Wunderlich B, Poland D. J Polym Sci (A) 1963;1:357–72.
[10] Richardson MJ, Flory PJ, Jackson JB. Polymer 1963;4:221–36.
[11] Bodily D, Wunderlich B. J Polym Sci 1966;A2:25.
[12] Baker CH, Mandelkern L. Polymer 1966;7:71–83.
[13] Kavesh S, Schultz JM. J Polym Sci (A-2) 1970;8:243–76.
[14] Preedy JE. Br Polym J 1973;5:13–9.
[15] Howard PR, Crist B. J Polym Sci (Phys) 1989;27:2269–82.
[16] Bunn CW. In: Renfrew A, Morgan P, editors. Polythene: the technology and uses of ethylene polymers, London: Iliffe, 1960. p. 87–130.
[17] Davis GT, Eby RK, Martin GM. J Appl Phys 1968;39:4973.
[18] Davis GT, Eby RK, Colson JP. J Appl Phys 1970;41:4316–26.
[19] Cutler DJ, Hendra PJ, Cudby MEA, Willis HA. Polymer 1977;18:1005–8.
[20] Vile J, Hendra PJ, Willis HA, Cudby MEA, Bunn A. Polymer 1984;25:1173–7.
[21] VanderHart DL, Pérez E. Macromolecules 1986;19:1902–9.
[22] Perez E, Vanderhart DL. J Polym Sci (Phys) 1987;25:1637–53.
[23] Perez E, VanderHart DL, Crist B, Howard PR. Macromolecules 1987;20:78–87.
[24] France C, Hendra PJ, Maddams WF, Willis HA. Polymer 1987;28:710–2.
[25] McFaddin DC, Russell KE, Kelusky EC. Polym Commum 1988;29:258–60.
[26] Perez E, Bello A, Perena JM, Benavente R, Martinez MC, Aguilar C. Polymer 1989;30:1508–12.
[27] Hosoda S, Nomura H, Gotoh Y, Kihara H. Polymer 1990;31:1999–2005.
[28] Hay JN, Zhou X-Q. Polymer 1993;34:1002–5.
[29] Russell KE, McFaddin DC, Hunter BK, Heyding RD. J Polym Sci (Phys) 1996;34:2447–58.
[30] Petraccone V, Allegra G, Corradini P. J Polym Sci (C) 1972;38:419–27.
[31] Reneker DH, Mazur J. Polymer 1988;29:3–13.
[32] Farmer BL, Eby RK. J Appl Phys 1974;45:4229–38.
[33] Farmer BL, Eby RK. Polymer 1979;20:363–6.
[34] Vonk CG. Colloid Polym Sci 1979;257:1021–32.
[35] Pakula T. Polymer 1982;23:1300–4.
[36] Pechhold W. Kolloid Z Z 1968;228:1–38.
[37] Balta Calleja FJ, Gonzalez Ortega JC, Martinez de Salazar J. Polymer 1978;19:1094–9.
[38] Heink M, Häberle K-D, Wilke W. Colloid Polym Sci 1991;269:675–81.
[39] Seguela R, Rietsch F. J Polym Sci, (Lett) 1986;24:29–33.
[40] Vonk CG. J Polym Sci (C) 1972;38:429–35.
[41] Kortleve G, Tuijnman CAF, Vonk CG. J Polym Sci (A-2) 1972;10:123–31.
[42] Vonk CG, Pijpers AP. J Polym Sci (Phys) 1985;23:2517–37.
[43] Wunderlich B. Macromolecular physics: volume 1. Crystal structure, morphology and Defects. New York: Academic Press, 1973.
[44] Scherr H, Pechhold W, Blasenbrey S. Kolloid Z Z 1970;238:396–405.
[45] Martinez de Salazar J, Balta Calleja FJ. J Cryst Growth 1979;48:283–94.
[46] Balta-Calleja FJ, Hosemann R. J Polym Sci (Phys) 1980;18:1159–65.
[47] Gaucher V, Seguela R. Polymer 1994;35:2049–55.
[48] Boyd RH. J Polym Sci 1975;13:2345–55.
[49] Wunderlich B. Polymer 1964;5:125.
[50] Holdsworth PJ, Keller A. Makromol Chem 1969;125:82–93.
[51] Wilke W, Vogel W, Hosemann R. Kolloid Z Z 1970;237:317–25.
[52] Hosemann R, Balta-Calleja FJ. Polymer 1979;20:1091–4.
[53] Napolitano R, Pucciariello R, Villani V. Macromol Theory Simul 1994;3:623–32.
[54] Tadokoro H. Structure of crystalline polymers. New York: Wiley, 1979.
[55] Corradini P, Petraccone V, Pirozzi B. Eur Polym J 1976;12:831–6.
[56] Corradini P. In: Ciardelli F, Giusti P, editors. Structural order in polymers, Oxford: Pergamon Press, 1981. p. 25–36.
[57] Sorensen RA, Liau WB, Kesner L, Boyd RH. Macromolecules 1988;21:200–8.
[58] Kusanagi H, Tadokoro H, Chatani Y, Suehiro K. Macromolecules 1977;10:405–13.
[59] Baker AME, Windle AH. Polymer 2000;42:651–65.
[60] Baker AME, Windle AH. Polymer 2000;42:667–80.
[61] Lipson H, Taylor CA. Fourier transforms and X-ray diffraction. London: Bell, 1958.
[62] Kawaguchi A, Ohara M, Kobayashi K. J Macromol Sci (Phys) 1979;B16:193–212.
[63] Phillips PJ, Tseng HT. Polymer 1985;26:650–4.
[64] Dorset DL. Polymer 1986;27:1349–52.
[65] Bonner JG, Frye CJ, Capaccio G. Polymer 1993;34:3532–4.
[66] Frye CJ. Personal communication, March 1996.
[67] Langford JI, Wilson AJC. J Sci Instrum 1962;39:581–5.
[68] Wiles DB, Young RA. J Appl Crystallogr 1981;14:149–51.
[69] Dollase WA. J Appl Crystallogr 1986;19:267–72.
[70] Hanna S, Windle AH. J Appl Crystallogr 1995;28:673–89.
[71] Hanna S, Baker AME, Windle AH. Polymer 1998;39:2409–14.
[72] International tables for X-ray crystallography. Birmingham: Kynock Press, 1968.
[73] Rappe AK, Casewit CJ, Colwell KS, Goddard WA, Skiff WM. J Am Chem Soc 1992;114:10024–35.
[74] Casewit CJ, Colwell KS, Rappe AK. J Am Chem Soc 1992;114:10 035–46.
[75] Rappe AK, Goddard WA. J Phys Chem 1991;95:3358–63.
[76] Fletcher R, Reeves CM. Comput J 1964;7:149.
[77] Axelson DE, Mandelkern L, Levy GC. J Am Chem Soc 1979;12:41.
[78] Hosemann R, Bagchi SN. Direct analysis of diffraction by matter. Amsterdam: North-Holland, 1962.
[79] Guinier A. X-ray diffraction in crystals, imperfect crystals, and amorphous bodies. New York: Dover, 1963.
[80] Hosemann R, Wilke W. Makromol Chem 1968;118:230–49.